Back-scattered detection provides atomic-scale localization precision, stability, and registration in 3D

Ashley R. Carter,[1] Gavin M. King, and Thomas T. Perkins[2*]

JILA, National Institute of Standards and Technology and University of Colorado, Boulder, Colorado 80309
[1]Department of Physics, University of Colorado, Boulder, Colorado 80309
[2]Department of Molecular, Cellular, and Developmental Biology, University of Colorado, Boulder, Colorado 80309
**Corresponding author: tperkins@jila.colorado.edu*

Abstract: State-of-the-art microscopy techniques (*e.g.*, atomic force microscopy, scanning-tunneling microscopy, and optical tweezers) are sensitive to atomic-scale (100 pm) displacements. Yet, sample drift limits the ultimate potential of many of these techniques. We demonstrate a general solution for sample control in 3D using back-scattered detection (BSD) in both air and water. BSD off a silicon disk fabricated on a cover slip enabled 19 pm lateral localization precision (Δf = 0.1–50 Hz) with low crosstalk between axes (≤3%). We achieved atomic-scale stabilization (88, 79, and 98 pm, in x, y, and z, respectively; Δf = 0.1–50 Hz) and registration (≈50 pm (rms), N = 14, Δt = 90 s) of a sample in 3D that allows for stabilized scanning with uniform steps using low laser power (1 mW). Thus, BSD provides a precise method to locally measure and thereby actively control sample position for diverse applications, especially those with limited optical access such as scanning probe microscopy, and magnetic tweezers.

OCIS codes: (180.0180) Microscopy; (180.6900) Three-dimensional microscopy; (120.0120) Instrumentation, measurement, and metrology; (180.5810) Scanning microscopy.

References and links

1. W. Denk and W. W. Webb, "Optical measurement of picometer displacements of transparent microscopic objects," Appl. Opt. **29**, 2382-2391 (1990).
2. G. Binnig, C. F. Quate, and C. Gerber, "Atomic Force Microscope," Phys. Rev. Lett. **56**, 930-933 (1986).
3. G. Binnig, H. Rohrer, C. Gerber, and E. Weibel, "7X7 Reconstruction on Si(111) Resolved in Real Space," Phys. Rev. Lett. **50**, 120-123 (1983).
4. N. H. Thomson, M. Fritz, M. Radmacher, J. P. Cleveland, C. F. Schmidt, and P. K. Hansma, "Protein tracking and detection of protein motion using atomic force microscopy," Biophys. J. **70**, 2421-2431 (1996).
5. L. Nugent-Glandorf, and T. T. Perkins, "Measuring 0.1-nm motion in 1 ms in an optical microscope with differential back-focal-plane detection," Opt. Lett. **29**, 2611-2613 (2004).
6. G. M. King and J. A. Golovchenko, "Probing nanotube-nanopore interactions," Phys. Rev. Lett. **95**, 216103 (2005).
7. D. M. Eigler and E. K. Schweizer, "Positioning single atoms with a scanning tunnelling microscope," Nature **344**, 524-526 (1990).
8. Y. Sugimoto, M. Abe, S. Hirayama, N. Oyabu, O. Custance, and S. Morita, "Atom inlays performed at room temperature using atomic force microscopy," Nature Materials **4**, 156-159 (2005).
9. E. E. Moon, M. K. Mondol, P. N. Everett, and H. I. Smith, "Dynamic alignment control for fluid-immersion lithographies using interferometric-spatial-phase imaging," J. Vac. Sci. Technol. B **23**, 2607-2610 (2005).
10. E. E. Moon and H. I. Smith, "Nanometer-precision pattern registration for scanning-probe lithographies using interferometric-spatial-phase imaging," J. Vac. Sci. Technol. B **24**, 3083-3087 (2006).
11. M. Capitanio, R. Cicchi, and F. S. Pavone, "Position control and optical manipulation for nanotechnology applications," Eur. Phys. J. B **46**, 1-8 (2005).
12. A. R. Carter, G. M. King, T. A. Ulrich, W. Halsey, D. Alchenberger, and T. T. Perkins, "Stabilization of an optical microscope to 0.1 nm in three dimensions," Appl. Opt. **46**, 421-427 (2007).

#86460 - $15.00 USD Received 14 Aug 2007; revised 17 Sep 2007; accepted 25 Sep 2007; published 28 Sep 2007

13. K. Visscher, S. P. Gross, and S. M. Block, "Construction of Multiple-Beam Optical Traps with Nanometer-Resolution Position Sensing," IEEE J. Sel. Top. Quantum Electron. **2**, 1066-1076 (1996).
14. M. E. J. Friese, H. Rubinsztein-Dunlop, N. R. Heckenberg, and E. W. Dearden, "Determination of the force constant of a single-beam gradient trap by measurement of backscattered light," Appl. Opt. **35**, 7112-7116 (1996).
15. J. H. G. Huisstede, K. O. van der Werf, M. L. Bennink, and V. Subramaniam, "Force detection in optical tweezers using backscattered light," Opt. Express **13**, 1113-1123 (2005).
16. U. F. Keyser, J. van der Does, C. Dekker, and N. H. Dekker, "Optical tweezers for force measurements on DNA in nanopores," Rev. Sci. Instrum. **77**, 105105 (2006).
17. U. F. Keyser, B. N. Koeleman, S. Van Dorp, D. Krapf, R. M. M. Smeets, S. G. Lemay, N. H. Dekker, and C. Dekker, "Direct force measurements on DNA in a solid-state nanopore," Nature Phys. **2**, 473-477 (2006).
18. J. M. Antonietti, J. Gong, V. Habibpour, M. A. Rottgen, S. Abbet, C. J. Harding, M. Arenz, U. Heiz, and C. Gerber, "Micromechanical sensor for studying heats of surface reactions, adsorption, and cluster deposition processes," Rev. Sci. Instrum. **78**, 054101 (2007).
19. J. R. Barnes, R. J. Stephenson, C. N. Woodburn, S. J. Oshea, M. E. Welland, T. Rayment, J. K. Gimzewski, and C. Gerber, "A Femtojoule Calorimeter Using Micromechanical Sensors," Rev. Sci. Instrum. **65**, 3793-3798 (1994).
20. K. C. Neuman, E. H. Chadd, G. F. Liou, K. Bergman, and S. M. Block, "Characterization of photodamage to Escherichia coli in optical traps," Biophys. J. **77**, 2856-2863 (1999).
21. T. T. Perkins, R. V. Dalal, P. G. Mitsis, and S. M. Block, "Sequence-dependent pausing of single lambda exonuclease molecules," Science **301**, 1914-1918 (2003).
22. J. Gelles, B. J. Schnapp, and M. P. Sheetz, "Tracking kinesin-driven movements with nanometre-scale precision," Nature **331**, 450-453 (1988).
23. J. Kohler, M. Albrecht, C. R. Musil, and E. Bucher, "Direct growth of nanostructures by deposition through an Si3N4 shadow mask," Physica E **4**, 196-200 (1999).
24. M. J. Lang, C. L. Asbury, J. W. Shaevitz, and S. M. Block, "An automated two-dimensional optical force clamp for single molecule studies," Biophys. J. **83**, 491-501 (2002).
25. F. Gittes, and C. F. Schmidt, "Interference model for back-focal-plane displacement detection in optical tweezers," Opt. Lett. **23**, 7-9 (1998).
26. A. Pralle, M. Prummer, E. L. Florin, E. H. K. Stelzer, and J. K. H. Horber, "Three-Dimensional High-Resolution Particle Tracking for Optical Tweezers by Forward Scattered Light," Microscopy Res. Tech. **44**, 378-386 (1999).
27. E. D. Palik, ed. *Handbook of optical constants of solids* (Academic Press, 1997).
28. W. H. Press, S. A. Teukolsky, W. T. Vetterling, and B. P. Flannery, *Numerical Recipes in C, The Art of Scientific Computing* (Cambridge University Press, 1992).
29. E. A. Abbondanzieri, W. J. Greenleaf, J. W. Shaevitz, R. Landick, and S. M. Block, "Direct observation of base-pair stepping by RNA polymerase," Nature **438**, 460-465 (2005).
30. D. W. Pohl, and R. Moller, "Tracking tunneling microscopy," Rev. Sci. Instrum. **59**, 840-842 (1988).
31. B. S. Swartzentruber, "Direct measurement of surface diffusion using atom-tracking scanning tunneling microscopy," Phys. Rev. Lett. **76**, 459-462 (1996).
32. M. Abe, Y. Sugimoto, T. Namikawa, K. Morita, N. Oyabu, and S. Morita, "Drift-compensated data acquisition performed at room temperature with frequency modulation atomic force microscopy," Appl. Phys. Lett. **90**, 203103 (2007).
33. C. R. K. Marrian, and E. S. Snow, "Proximal probe lithography and surface modification," Microelectron. Eng. **32**, 173-189 (1996).
34. M. Radmacher, M. Fritz, H. G. Hansma, and P. K. Hansma, "Direct observation of enzyme activity with the atomic force microscope," Science **265**, 1577-1579 (1994).
35. D. J. Muller, K. T. Sapra, S. Scheuring, A. Kedrov, P. L. Frederix, D. Fotiadis, and A. Engel, "Single-molecule studies of membrane proteins," Curr. Opin. Struct. Biol. **16**, 489-495 (2006).

1. Introduction

Atomic-scale sensing lies at the heart of a variety of microscopies with high positional precision [1-3]. Yet, such high sensitivity without similar stability limits the utility of these techniques [4-6]. For instance, a scanning probe microscope (SPM) image should be composed of a series of pixels with uniform and repeatable spacing. This requires excellent scanning. Returning to a particular feature in a scanned image requires excellent registration. Holding that feature stationary to deduce its time-dependent dynamics requires excellent stability. Thus, there is a clear need for sample control with atomic-scale (100 pm) positional precision, registration, and stability. While such a combination of positional precision, stability, and registration has been achieved passively in SPM at cryogenic temperatures [7] and in ultrahigh vacuum [8], there is no routine method to achieve this triumvirate of requirements in air or fluid at room temperature.

#86460 - $15.00 USD Received 14 Aug 2007; revised 17 Sep 2007; accepted 25 Sep 2007; published 28 Sep 2007

Several existing methods address active sample control with varying success. Commercial, closed-loop piezo-electric (PZT) stages provide for precise relative motion. Such stages rely on capacitive sensors to maintain stability of the stage with respect to its frame, though these sensors are often located many centimeters away from the measurement position. Sample drift occurs due to perturbations unseen by the capacitive sensors. What is needed is a *local*, high-bandwidth sensor of sample drift with excellent positional precision. Then, a PZT stage would generate displacements that compensate for the locally measured drift. One implementation of this general method uses an optical grating as a sensor for both lithographic [9] and, more recently, atomic force microscope (AFM) applications [10]. But, such gratings and their accompanying optics are cumbersome, often are not local to the measurement point, and do not achieve atomic-scale stabilities, but rather stabilities of 0.28 nm, 0.39 nm, and <1 nm in *x*, *y*, and *z*, respectively [10]. Video tracking of affixed micron-sized beads achieves stabilities of 0.8 nm [11], though such affixed beads do not necessarily reflect the motion of the sample at the level of 100 pm [12].

We have previously demonstrated 100-pm sample stabilization in 3D for optical microscopes and optical-trapping assays [12]. Since that work used forward-scattered detection (FSD) [13], it is not compatible with SPM or magnetic tweezers applications due to limited or poor quality optical access opposite of the imaging objective. Back-scattered detection (BSD), initially demonstrated over 10 years ago for optically trapped beads [14], has recently been investigated with renewed interest [15, 16]. For instance, Huisstede *et al.* elegantly demonstrated that position-sensitive detectors provide enhanced lateral detector range over quadrant photodiodes (QPD) [15]. Additionally, Keyser *et al.* measured the vertical motion of an optically trapped bead to ~5 nm positional precision with BSD [16, 17]. To demonstrate application of BSD to techniques beyond optical trapping, we focus on the general issue of sample control in 3D. We see three critical criteria to demonstrate before BSD is adopted for sample control in SPM and other applications. These criteria are: (*i*) atomic-scale localization precision in 3D, (*ii*) similar-scale stability in 3D, and (*iii*) low optical crosstalk between detection axes. Achieving these criteria leads to excellent registration.

In this report, we demonstrate the first BSD optical signals from silicon disks in both air and water. Silicon disks led to enhanced sensitivity when compared to equal volume polystyrene beads. BSD off these disks also offered low crosstalk between axes (*x*-*y* coupling of ≤3% and *x*-*z* coupling of ≤1%). Additionally, we achieved both atomic-scale stabilization and registration in 3D with low laser power (1 mW). Thus, BSD provides a general and highly precise method for detecting and thereby actively controlling local sample position in 3D for diverse applications including SPM, magnetic tweezers, and optical-trapping assays.

2. Materials and methods

2.1 Experimental apparatus

We achieved precise sample control using a local measurement of sample position coupled with a careful reduction of noise sources (*e.g.*, optical, acoustical, thermal, and mechanical). The BSD signal arises from scattering a laser off a silicon disk (r = 250 nm, h = 56 nm; see Section 2.2). The laser was focused and the back-scattered light was collected using a single high numerical aperture (NA) objective (Nikon, PlanAPO-100X-IR, NA=1.4) [Fig. 1(a)].

BSD often suffers from inefficient use of light (0.02-0.1%) [15], with prior work separating BSD signals from the incident light via partially reflective mirrors that decreased the power of both the incident and BSD light [15-17]. Low BSD laser power minimizes potential perturbation in future applications. For instance, when measuring the position of a metal-coated AFM cantilever in vacuum, deflection due to laser heating can be substantial (~1 nm/μW) [18, 19]. Thus, we sought to minimize laser noise while maximizing the efficiency of photon collection [Fig. 1(b)]. To do so, an 810-nm stabilized diode laser (SDL) was directed into the back of a microscope objective using a dichroic mirror [12]. Efficient collection of the

#86460 - $15.00 USD Received 14 Aug 2007; revised 17 Sep 2007; accepted 25 Sep 2007; published 28 Sep 2007

back-scattered signal was achieved using an optical isolator, which consisted of a polarizing beam splitter (PBS) and a quarter-wave plate (λ/4). We further increased this efficiency by underfilling our 10-mm diameter quadrant photodiode (QPD) with a 6-mm back-scattered beam, in contrast to previous experiments that used an overfilled QPD [14] or BSD in combination with a reflective element [16, 17] to deduce vertical position. As a result, with only 1.3 mW incident upon the objective (and 60% of that at the sample [20]), we achieved a high collection efficiency (5%) of the input light at the QPD (YAG 444-4A, PerkinElmer Optoelectronics). This efficiency enabled us to use low laser power (800 μW at the laser focus) while achieving high sensitivity in all three axes over a broad range of frequencies (see Section 3.2).

The resulting QPD voltages were amplified using custom-built electronics and digitized. The sample's position was then controlled via a software-based feedback loop using a closed-loop, piezo-electric stage (P733.3DD, PI). This direct-drive stage allowed for millisecond response times. The stage was also used to calibrate the QPD positional response (see Section 2.3). During active stabilization, the optical signal detected sample position and the stage was used within a feedback loop to minimize unwanted motion.

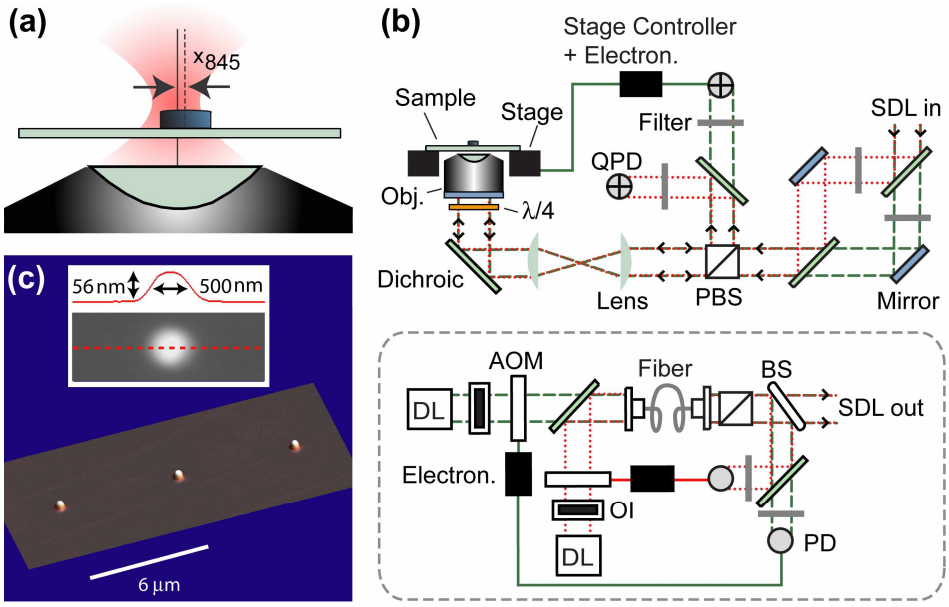

Fig. 1. (a). Schematic showing a focused laser beam interacting with a silicon fiducial mark (*not to scale*). (b) Optical layout for back-scattered detection (BSD). Two diode lasers [λ = 810 nm (*green dashed line*), 845 nm (*red dotted line*)] were actively stabilized by the combination of optics shown in the gray box, see [12]. These stabilized diode lasers (SDL) were simultaneously launched from a single fiber. Each laser was independently translated in the imaging plane by mirrors conjugate to the objective's (Obj.) back aperture. The combination of the polarizing beam splitter (PBS) and quarter-waveplate (λ/4) led to highly efficient BSD. Acronyms represent the following: diode laser (DL), optical isolator (OI), acousto-optic modulator (AOM), photodiode (PD), beam sampler (BS), and quadrant photodiode (QPD). Blue-shaded components are in optically conjugate planes. (c) Atomic force microscope image showing an array of three silicon disks (radius, r = 250 nm; height, h = 56 nm). Inset: line scan across a disk.

In the ultimate application of sample control by BSD, we anticipate stabilizing the sample with respect to another object (*i.e.*, an AFM tip, a bead, or a lithographic mask) detected by a

#86460 - $15.00 USD Received 14 Aug 2007; revised 17 Sep 2007; accepted 25 Sep 2007; published 28 Sep 2007

second laser. We therefore introduced an additional SDL (λ = 845 nm) that by design shares a largely co-linear beam path with the initial laser. Independent control of both lasers in the sample plane was achieved with a mirror in a conjugate plane to the back focal plane of the objective. Common-mode noise (*e.g.*, mechanical motion of the fiber tip) was suppressed in this differential measurement scheme [5]. Thus, the differential stability between the lasers will be the ultimate limitation [19 pm laterally, 73 pm vertically, Δf = 0.1–50 Hz, see Section 3.2]. In the present work, we used the second laser as an "out-of-loop" monitor to verify sample stabilization in this differential coordinate system between the laser foci – the coordinate system to be used in future applications.

Our experimental apparatus exhibited extremely low-noise characteristics because of careful reduction in mechanical, environmental, and optical noise. The instrument consisted of an inverted optical microscope frame modified for increased stiffness [5]. Both the PZT stage and the sample were custom-mounted, as described previously [5, 12]. The sample consisted of a cover slip in an epoxy-stabilized flow cell [21] filled with water, unless otherwise noted. Three layers of environmental isolation were used: (*i*) optics external to the microscope were enclosed in a box; (*ii*) the whole assembly was enclosed by a custom-built, acoustically isolated box; and (*iii*) the experiment was mounted on a research grade optical table. Optical noise was actively minimized via a combination of components that reduced pointing, mode, intensity, and polarization noise (Fig. 1(b), *gray dashed box*) [12].

2.2 Silicon disk fabrication

Silicon disks are superior fiducial marks for BSD. Previously, we and others have used polystyrene beads affixed to the cover slip as fiducial marks [5, 11, 22]. But, these beads do not necessarily reflect sample motion on distances of ~100 pm [12]. Fiducial marks engineered into cover slips (*e.g.*, nanofabricated glass posts) overcome this limitation [12] and are compatible with standard fabrication techniques. Yet, such glass posts were serially exposed in an electron beam (e-beam) and required deposition of resist over the entire cover slip. Here, we developed protocols for parallel fabrication of silicon disks along with efficient reuse of these customized cover slips. Our parallel fabrication only locally deposits silicon on the cover slips and thus does not degrade or alter the overall surface chemistry, which is important in biological applications. Moreover, the surface of the deposited silicon rapidly oxidizes, forming a biologically compatible interface.

We fabricated 1 mm^2 arrays of silicon disks in a 6-μm grid [Fig. 1(c)] on clean glass cover slips via physical vapor deposition of silicon through a silicon-nitride shadow mask [23]. Mask fabrication began by spinning e-beam resist (ZEP-520, Zeon) onto 200-nm thick, 2 × 2 mm silicon-nitride membrane windows (Silson). The resist was then exposed via e-beam lithography (38 keV, 15 pA, 50 $\mu C/cm^2$) and developed. Holes were then etched through the window in a reactive ion etcher (CF_4, 16 sccm, 20 Pa, 100 W, 90 s). Next, 3-μm-tall standoffs were fabricated around the perimeter of the patterned window via optical lithography with SU-8 (Microchem). Prior to depositing silicon, the glass cover slips were cleaned in ethanolic 10 M potassium hydroxide. Finally, silicon was deposited through the shadow mask in an evaporation chamber (0.1 nm/s, 1×10^{-4} Pa). The diameter and height of the silicon disks were measured by AFM with a high aspect ratio tip (STING tip, MikroMasch). One general advantage of physical vapor deposition through a shadow mask is that the material composition (and thus the index of refraction) of the disks is highly tunable. Additionally, by using four shadow masks in parallel, four cover slips were made per 30-min. cycle, where cycle time was limited by evaporator pumping time. Cover slips were recovered and cleaned after use by immersing them in sulfuric acid and hydrogen peroxide (50:1, 80 ˚C). Surface chemistry after such cleaning was compatible with single-molecule biophysics experiments.

#86460 - $15.00 USD Received 14 Aug 2007; revised 17 Sep 2007; accepted 25 Sep 2007; published 28 Sep 2007

2.3 Data acquisition

The fiducial mark's horizontal motion (x, y) relative to the laser was deduced from the intensity difference on the QPD, while vertical motion (z) was deduced by the sum signal, which is the total light falling upon the four quadrants of the QPD. To improve localization precision, lateral signals were amplified from the normalized difference signals and the vertical signals were offset amplified [12] to better match the 20-volt range on the 18-bit data acquisition card (M-series, National Instruments). After antialiasing, signals were digitized at 4 kHz and converted to position using calibration curves similar to those shown in Fig. 2, *thick lines*. This yielded two sets of positions deduced separately from each laser (*e.g.*, x_{845}, y_{845}, and z_{845}).

During active stabilization, the average sample position was measured with the 810-nm laser every 10 ms and used to generate a proportional error signal to the stage controller (E-710.P3D, PI). We used the position signals from the 845-nm laser to verify sample stabilization. The resulting records were low-pass filtered (smoothed and decimated) to 10 Hz for presentation, except where noted.

3. Results

Future ultrastable scanning applications demand active atomic-scale control of the sample position. After first establishing the high sensitivity of BSD (Section 3.1) and its superior stability and localization precision (Section 3.2), we then demonstrate the utility of BSD with stabilized scans of a sample surface (Section 3.3). Stabilized scans, composed of orthogonal steps, allow averaging during imaging, and hence a higher signal-to-noise (S/N) ratio. Registration during scanning is also maintained to ≈50 pm (rms) (Section. 3.4), even after many 100-nm displacements (N = 14).

3.1 Sensitivity

We first needed to investigate the sensitivity limits for BSD. To do so, we sequentially scanned the silicon disks through the laser focus in all three axes using the PZT stage and recorded the resulting QPD signals (Fig. 2, *thick lines*). This yielded sensitivities of 38 mV/nm, 40 mV/nm, and 20 mV/nm in x, y, and z, respectively, sufficient for detecting ~2–4 pm motion using an 18-bit data card over a 20-volt range. Thus, BSD has the sensitivity to detect single-picometer motion, though our achieved localization precision limit (19 pm) is currently limited by other noise sources (see Section 3.2).

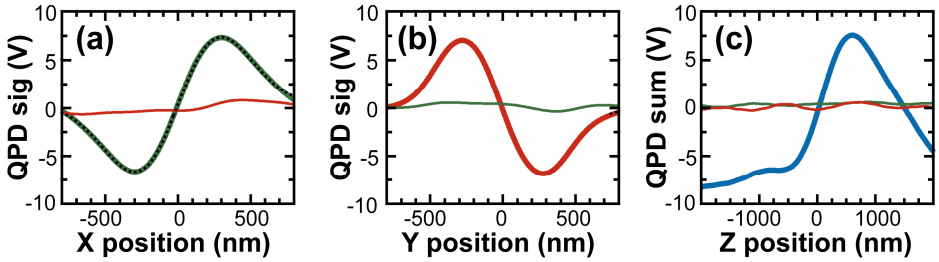

Fig. 2. Sensitivity of BSD signals. Records were measured while moving on one axis (*thick line*) while simultaneously measuring the off-axis response (*thin line*). Signals in x, y, and z are represented by *green*, *red*, and *blue*, respectively. (a) Motion in x. The lateral response was well fit by the derivative of a Gaussian (*dashed line*). (b) Motion in y. (c) Motion in z.

Motion in one axis that leads to an optical signal on an orthogonal axis complicates detection. Thus, we sought to minimize such optical crosstalk between axes. This required careful optical adjustments including: (*i*) independent angular and lateral alignment of the beam on the back-aperature; (*ii*) rotations of the quarter waveplate and of the QPD; and (*iii*)

#86460 - $15.00 USD Received 14 Aug 2007; revised 17 Sep 2007; accepted 25 Sep 2007; published 28 Sep 2007

fixing the mounting angle of the quarter waveplate such that back reflections off it did not enter the QPD. Crosstalk was also minimized by precisely centering the silicon disk relative to the laser beam using an automated routine. This centering was achieved by fitting the lateral response along the horizontal axes to the derivative of a Gaussian (Fig. 2(a), *dashed line*). By these procedures, we achieved a low level of crosstalk: 3% between *x* and *y* signals and 1% between lateral and *z* signals over a 200-nm region (Fig. 2), similar to the results achieved in FSD [24]. For raster-scanning applications, increased accuracy, or for large displacements, we parameterized the residual crosstalk [24].

BSD's high sensitivity (*S*) is not limited to silicon (Si) disks. We directly compared these disks (Fig. 3, *green*) to polystyrene (ps) beads (Fig. 3, *red*) at equal amplification and without vertical offset amplification. The resulting records showed comparable BSD signals for polystyrene beads (r = 300 nm). This comparable lateral sensitivity (S_{Si}/S_{ps} = -0.8) was achieved even though the beads were 10-fold larger by volume than the disks; the sign change in S_{PS} for small polystyrene beads has previously been reported [15].

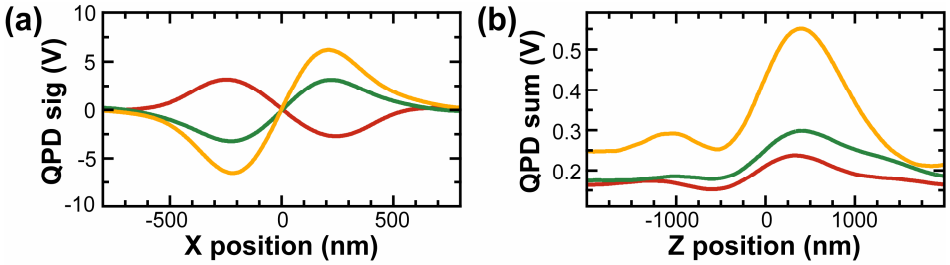

Fig. 3. BSD signals vary with the index of refraction of the medium and the fiducial mark. Comparison between silicon disks in water (*green*) and air (*gold*), with polystyrene beads (r = 300 nm) in water (*red*) for both lateral (a) and vertical (b) sensitivity.

Qualitatively, we would expect a larger sensitivity per unit volume to arise from silicon's higher index of refraction. To test this hypothesis, we compared the induced dipole moment for both silicon disks and polystyrene beads. Gittes and Schmidt have successfully applied a first-order interference model to quantitatively predict the detector response for FSD by spherical beads in the Rayleigh approximation [25]. These authors and others [26] have shown that the magnitude of the detector response scales with the polarizability α of the scattering particle. We applied this approximation to the observed lateral back-scattered signals. Thus, the polarizability of spherical scattering particles is:

$$\alpha_{sphere} = \left[\frac{m^2 - 1}{m^2 + 2}\right]\frac{3V}{4\pi}, \tag{1}$$

where V is the volume, and m is the index of refraction ratio ($m = n_{object} / n_{solvent}$) [25]. This equation holds for the general case of complex m. By approximating the silicon disk as a sphere and using an index of 3.9 + 0.15i (amorphous silicon at λ = 810 nm) [27], we calculated the ratio of the polarizability between silicon and polystyrene to be:

$$\frac{|\alpha_{Si}|}{|\alpha_{ps}|} = \frac{V_{Si}}{V_{ps}}\left[\frac{\frac{m_{Si}^2 - 1}{m_{Si}^2 + 2}}{\frac{m_{ps}^2 - 1}{m_{ps}^2 + 2}}\right] = \frac{V_{Si}}{V_{ps}}[7.1], \tag{2}$$

The measured ratio of sensitivities and thus, within our approximation, the ratio of polarizabilities is 0.8. After division by 7.1, this yields a predicted volume ratio of 0.11 in agreement with the actual volume ratio of 0.10. Thus, within this approximation, we showed

#86460 - $15.00 USD Received 14 Aug 2007; revised 17 Sep 2007; accepted 25 Sep 2007; published 28 Sep 2007

that the increased lateral sensitivity of silicon relative to polystyrene is consistent with silicon's higher index of refraction. As a consequence, by using silicon, we could use substantially smaller fiducial marks while retaining suitable sensitivity.

We note that the success of this first-order approximation does not prove the lateral sensitivity is linear in α nor that an interference model is the correct description of BSD. However, like the interference model for FSD [25], our lateral response is quantitatively described by the derivative of a Gaussian (Fig. 2(a), *dashed line*). Our 500-nm diameter, 56-nm high disks are neither large nor small compared to the wavelength of light and, therefore, the Rayleigh (or Mie) approximation is not strictly correct. Future work, based upon a detailed study of the response for both silicon disks and polystyrene beads as a function of their size and surrounding medium, coupled with improved modeling, should lead to a complete description of BSD.

Vertical response of BSD is distinctly different than that of FSD. For BSD, there is a small baseline offset in the sum signal (0.15 V). As the disk was vertically scanned through the beam waist (Fig. 3(b), *green*), the scattered light dramatically increased 200% to a maximum and then monotonically decreased towards the baseline over ~1500 nm (maximal lateral sensitivity occurs at $z \approx 0$). In contrast, vertical motion in FSD leads to a small modulation (~10%) on top of a comparatively large static signal [26]. We also note that the origin of our BSD vertical sensitivity was different than prior BSD reports; we underfilled our 10-mm diameter QPD with a 6-mm beam, whereas prior vertical sensitivity was based on overfilling the QPD [14] or using BSD in combination with a reflective element [16, 17].

One application of this work is in scanning and stabilizing a sample for SPM; many SPM applications occur in air or vacuum. To demonstrate BSD in air (Fig. 3, *gold*), we scanned the silicon disk through the detector beam in the flow chamber, prior to measuring the same disks in water. The sensitivities were higher in air than in water. Thus, these records show BSD is compatible with SPM application in non-aqueous environments.

Overall, BSD detection provides excellent optical signals for both polystyrene beads and silicon disks, and is capable of sensing very small motions with minimal crosstalk. Lateral response was well fit by the derivative of a Gaussian and is similar in shape to the FSD response. Vertical response was distinctly different and inherently more sensitive than the FSD response.

3.2 Stabilization and localization precision

For a potential ultrastable SPM and many other applications, a prerequisite for excellent registration is comparable stability. To demonstrate such control, we next actively stabilized our stage with one laser beam while measuring the residual motion with the second laser [Fig. 4(a)]. We achieved average short-term stabilities of $\bar{\sigma}_x$ = 48 pm, $\bar{\sigma}_y$ = 48 pm, and $\bar{\sigma}_z$ = 49 pm. These stabilities were calculated by taking the standard deviation of the data low-pass filtered to 25 Hz within a 1 s interval and averaging 100 such non-overlapping intervals. We also achieved a long-term stability of σ_x = 50 pm, σ_y = 49 pm, and σ_z = 57 pm by calculating the standard deviation of 100 s of data filtered at 25 Hz.

While previous experiments using BSD do not report real-space stabilities, they do report power spectral density (PSD) for their *electronic* noise floor [14, 15]. In Fig. 4(b), we plot the PSD of our actual stabilization records. At higher frequencies (>20 Hz), our achieved stabilities were equal to or better than these previous electronic noise floors. At low frequencies (<20 Hz), our achieved stabilities stayed low; previous BSD work, in contrast, showed a rapidly increasing electronic noise floor as well as a 2-fold increase in the PSD of an optically trapped bead between 20 and 2 Hz, suggesting significant low frequency noise [15]. Our low broadband noise (~10 pm/$\sqrt{\text{Hz}}$ between 0.1 Hz and 1 kHz) demonstrates the significant reduction in instrumental noise achievable with BSD coupled with active reduction in optical and mechanical noise.

#86460 - $15.00 USD Received 14 Aug 2007; revised 17 Sep 2007; accepted 25 Sep 2007; published 28 Sep 2007

An excellent alternative metric for calculating stabilities is to integrate the PSD within a specified bandwidth. We computed the integrated noise from 0.1 to 50 Hz, a broad bandwidth useful for a range of SPM and optical trapping experiments. The resulting stabilities were 88, 79, and 98 pm, in *x*, *y*, and *z* respectively. Calculating the equivalent metric on real-space data yields similar results as required by Parseval's Theorem [28], verifying the appropriate scaling of the PSD. Thus, our stability over this real-world useful bandwidth (0.1-50 Hz) is at or below 100 pm on all three axes.

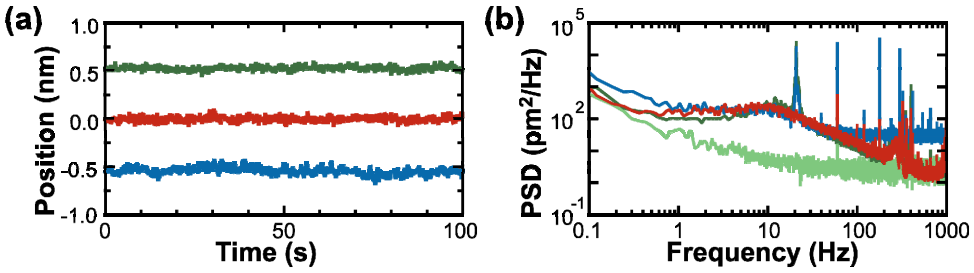

Fig. 4. Active 3D stabilization. (a) Sample position as measured by the 845-nm laser: x_{845} (*green*), y_{845} (*red*), and z_{845} (*blue)*. Positions determined with the 810-nm laser were used for feedback (*not shown*). (b) Power spectral densities (PSD) of the stabilized data shown in (a) (*red*, *green*, and *blue*). Our lateral localization precision limit, deduced by measuring the same unstabilized disk with two lasers [5], was substantially lower (*light green*).

The origin of BSD's stability and one potentially significant advantage over FSD is its optical conciseness, which leads to better mechanical stability. Mechanical stability enables the substantial, yet zero mean, Brownian motion inherent in many assays to be averaged down to atomic dimensions. This is an engineering challenge in FSD since it requires excellent mechanical stability at two different vertical levels — that of the input light coupled into the objective and that of the output light on the back side of the condenser incident upon the QPD. For inverted microscopes, this second vertical level is the more technically challenging one; it requires a lightweight, mechanically rigid set of lenses, filters, and QPDs that is often bolted onto the condenser arm of a commercial research microscope. In contrast, in BSD, the optics external to the microscope are in a single horizontal plane.

Achieved stabilities do not reflect the ultimate localization precision of BSD. A better metric is the differential detection of a common signal by both lasers [5]. More specifically, two lasers measure the same object; the difference reflects the uncertainty in the measurement. Our average, short-term (1s), differential stability, measured without stabilization, was ~4-fold lower laterally ($\bar{\sigma}_x$ = 12 pm, $\bar{\sigma}_y$ = 11 pm, and $\bar{\sigma}_z$ = 38 pm) than our active stabilization results; this difference is also quite noticeable by plotting the PSD of our lateral localization precision limit (Fig. 4(b), *light green*). The integrated noise on the differential signal from 0.1 to 50 Hz was 19 pm in both *x* and *y*, and 73 pm in *z*.

Improvements in instrumentation to extend sample stabilization to this localization precision might include better mechanical and optical design as well as enhanced isolation from floor-borne vibrations (Fig. 4(b), 23-27 Hz *peak*). Low frequency performance can be limited by a number of factors, including non-common-mode optical-mechanical noise (*e.g.*, differential motion between the QPDs or mirrors), variations in index of refraction [29], and thermal stability. We speculate that our low frequency performance is currently limited by the temperature (>1°C) and pressure fluctuations in the room, which could be alleviated by moving the apparatus to a temperature regulated (0.2°C), acoustically quiet (NC30) room. High frequency performance is currently limited by our software-based feedback loop (100 Hz). Real-time embedded control (e.g. field programmable gate array) provides a means for deterministic timing and increased bandwidth up to and limited by the PZT stage resonance (1

#86460 - $15.00 USD Received 14 Aug 2007; revised 17 Sep 2007; accepted 25 Sep 2007; published 28 Sep 2007

kHz). For anticipated SPM applications, the loop closure time will limit the scan-rate for stabilized scans, while low frequency noise will limit registration and the ability to "hover" a tip over a specified point on the sample.

3.3 Ultrastable scanning and uniform steps

Ultrastable scanning of a sample requires precise steps. Ideally, such scanning would occur without drift on any axis. Atom tracking [30], the most popular method for sample stabilization in SPM [4, 31], is fundamentally incompatible with simultaneous stabilization and scanning. However, it is used in a feedforward sense by assuming constant drift velocities, which is most effective in ultrahigh vacuum [32]. In this work, we demonstrate simultaneous scanning and stabilization using BSD to locally measure and thereby control sample location. The basis of scanning is a series of uniform steps. To demonstrate uniformity in the step size, we made a staircase of 0.5-nm steps sequentially in all three axes. The sample position was actively controlled in 3D at all times with the 810-nm laser. Changes in the feedback set point led to scanning. The reported results were determined with the 845-nm laser, which provides an "out-of-loop monitor" of servo-performance. The resulting records show linear motion in one axis with negligible motion on the stationary axes [Fig. 5(a)].

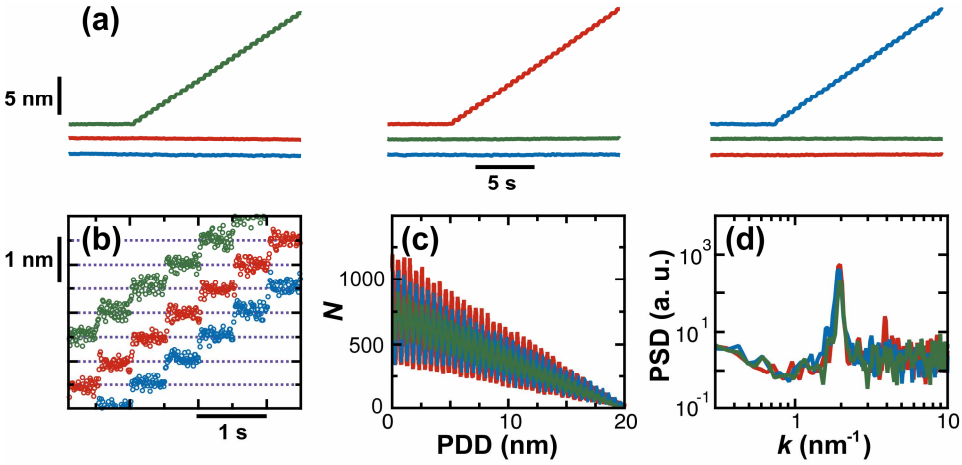

Fig. 5. Ultrastable scanning and uniform stepping. (a) The sample was moved in 0.5-nm steps sequentially along each axis under active stabilization. Sample position, independent of the servo-loop, was measured with the 845-nm laser [x_{845} (*green*), y_{845} (*red*), and z_{845} (*blue)*]. Traces displaced for clarity. (b) Individual steps low-pass filtered to 100 Hz show uniform 0.5 nm motion. Traces displaced for clarity. (c) A histogram of pairwise distance differences (PDD) along each axis shows peaks every 0.5 nm. (d) Fourier transform of the PDD histograms in (c) reveals the power spectral density (PSD) of the data. The peak of the PSD is at 2 nm^{-1}, as expected.

Individual steps were clearly resolved and repeatable in size in records low-pass filtered to 100 Hz [Fig. 5(b)]. To provide an unbiased measurement of step size and an estimate of the *S*/*N* ratio, we computed the pair-wise distance difference (PDD) [Fig. 5(c)], which calculates the distance between each pair of points [22]. Ideally, every such difference would be a multiple of 0.5 nm. A Fourier transform of the PDD histogram determines the spatial frequency components present in the data [Fig. 5(d)]. Peaks occurred at $k_x = 2.0 \pm 0.1$ nm^{-1}, $k_y = 1.9 \pm 0.1$ nm^{-1}, and $k_z = 1.9 \pm 0.1$ nm^{-1} (peak ± FWHM). The *S*/*N* ratio for these 0.5-nm steps is 30, 28, and 32, for motion along *x*, *y*, and *z*, respectively, based on the next largest peak in the PSD. Thus, our implementation of BSD enables both precise and accurate steps as well as scanning concurrent with active stabilization on all axes.

#86460 - $15.00 USD Received 14 Aug 2007; revised 17 Sep 2007; accepted 25 Sep 2007; published 28 Sep 2007

3.4 Registration

Precision is fundamental to registration — the ability to repeatedly return to a particular sample position. Sample drift limits registration. Excellent registration improves the repeatability of image acquisition and enables returning to a particular location in that image for subsequent detailed study. To demonstrate registration, we repeatedly moved the sample back and forth in 100-nm steps individually on all three axes for a total of fifteen 6-s long cycles [Fig. 6(a)]. The average step position (x_{845}^{n}) for each step back to the starting location was compared to the initial step value ($\Delta x^{n} = x_{845}^{n} - x_{845}^{0}$) and plotted versus the step number to show the spread in the relative registration [Fig. 6(b)]. The standard deviations of the relative position of these steps were 25 pm, 21 pm, and 58 pm in *x*, *y*, and *z*, respectively. The experiment was repeated with 1-nm steps and yielded essentially identical results. Thus, the registration is near to and limited by our long-term, low-frequency stability (σ_x = 11 pm, σ_y = 16 pm, σ_z = 40 pm, in 100 s of data filtered to 0.3 Hz).

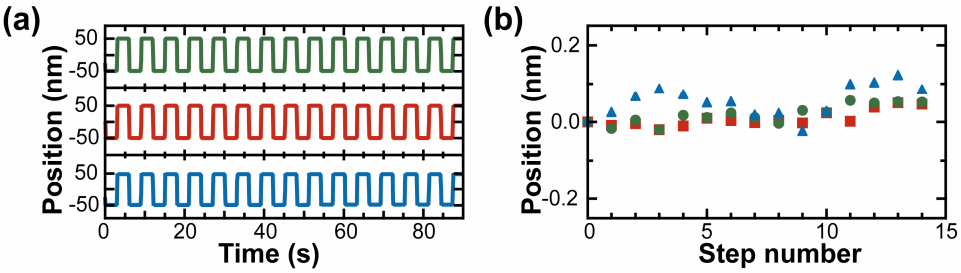

Fig. 6. Registration. (a). The sample was moved in a series of fifteen back-and-forth 100-nm steps sequentially on each axis. The steps were actively stabilized with the 810-nm laser while the resulting motion was verified with the 845-nm laser [x_{845} (*green*), y_{845} (*red*), and z_{845} (*blue)*]. (b) Mean values of step position around the starting location as a function of step number demonstrates excellent registration.

4. Conclusion

With BSD, we achieved atomic-scale (100 pm) sample localization precision, stability, and registration in all three axes. Moreover, we demonstrated that BSD can meet or exceed the best stabilities achieved with FSD in all dimensions. BSD also yields a 20-fold larger response to vertical motion than FSD. In contrast to prior BSD work, we achieved this enhanced vertical sensitivity when underfilling the QPD. Our lateral localization precision limit was 19 pm. Fundamental to this set of state-of-the art metrics, unprecedented in aqueous or ambient conditions, is active stabilization based on a local optical measurement of sample position. Thus, we could scan while actively stabilizing the sample on all three axes.

The optical and mechanical conciseness of BSD makes this technique amenable to a wide variety of applications and underlies its superior stability and optical efficiency. We foresee BSD's integration into many applications seeking ultrastable 3D detection and control, especially those with poor quality or limited optical access opposite of the microscope objective, such as SPM and magnetic tweezers. The scanning range can be easily extended to several microns by sequential moves of the detector beam with a PZT mirror. Silicon wafers, in lieu of cover glass, can be accommodated by shifting to a longer wavelength detector laser below silicon's band-gap.

Achieving active tip-sample control at atomic length scales would benefit diverse SPM applications ranging from proximal probe lithography [33] to direct interrogation of enzymatic turnover [34] to studies of protein structure [35]. Our success with sample control based on BSD signals from silicon disks suggests that a similar degree of control might be achieved by BSD off an SPM tip. We envision that one laser would control the sample

#86460 - $15.00 USD Received 14 Aug 2007; revised 17 Sep 2007; accepted 25 Sep 2007; published 28 Sep 2007

position and a second laser would control the tip position. Thus, this work is a necessary step towards and holds the promise of an ultra-stable SPM operating at room temperature in a plurality of environments.

Acknowledgments

This work was supported by separate Burroughs Wellcome Fund Career Awards to GMK and TTP, a National Research Council Research Associateship (GMK), an Optical Science and Engineering Program NSF-IGERT Grant (ARC), a National Physical Science Consortium Fellowship (ARC), a PI NanoInnovation Grant (ARC), the National Science Foundation (Phy-0404286 and Phy-1551010) and NIST. Mention of commercial products is for information only; it does not imply NIST's recommendation or endorsement. TTP is a staff member of NIST's Quantum Physics Division.

#86460 - $15.00 USD Received 14 Aug 2007; revised 17 Sep 2007; accepted 25 Sep 2007; published 28 Sep 2007